Optical and structural investigations on titanium oxynitride films for visible-UV photocatalytic applications

doi: 10.1063/1.5143609

Journal of Applied Physics

Optical and structural investigations on titanium oxynitride films for visible-UV photocatalytic applications

Cite as: J. Appl. Phys. **127**, 135301 (2020); https://doi.org/10.1063/1.5143609
Submitted: 26 December 2019 . Accepted: 17 March 2020 . Published Online: 02 April 2020

Jun Mizushiro, Kohei Yoshimatsu, Naoki Ohashi, Masahiko Tanaka, Osami Sakata, and Akira Ohtomo

Journal of Applied Physics ARTICLE scitation.org/journal/jap

Optical and structural investigations on titanium oxynitride films for visible-UV photocatalytic applications

Cite as: J. Appl. Phys. **127**, 135301 (2020); doi: 10.1063/1.5143609
Submitted: 26 December 2019 · Accepted: 17 March 2020 ·
Published Online: 2 April 2020

Jun Mizushiro,[1] Kohei Yoshimatsu,[1] Naoki Ohashi,[2,3,4] Masahiko Tanaka,[5] Osami Sakata,[4,6] and Akira Ohtomo[1,4,a)]

AFFILIATIONS

[1]Department of Chemical Science and Engineering, Tokyo Institute of Technology, 2-12-1 Ookayama, Meguro-ku, Tokyo 152-8552, Japan
[2]National Institute for Materials Science (NIMS), 1-1 Namiki, Tsukuba 305-0044, Japan
[3]Department of Applied Science for Electronics and Materials, Kyushu University, 6-1 Kasuga-Kouen, Kasuga, Fukuoka 816–8580, Japan
[4]Materials Research Center for Element Strategy (MCES), Tokyo Institute of Technology, Yokohama 226–8503, Japan
[5]Synchrotron X-ray Station at SPring-8, National Institute for Materials (NIMS), Sayo, Hyogo 679-5148, Japan
[6]Synchrotron X-ray Group, Research Center for Advanced Measurement and Characterization, National Institute for Materials (NIMS), Sayo, Hyogo 679-5148, Japan

[a)]**Author to whom correspondence should be addressed:** aohtomo@apc.titech.ac.jp

ABSTRACT

We report on the epitaxial growth of titanium oxynitride (TiO_xN_y) films on α-Al_2O_3 (0001) substrates by using a pulsed-laser deposition technique and their optical properties. Using TiN as a solid source, N content (y) in the films was tuned by changing the partial pressure of O_2 gas. The crystalline phase was found to evolve up to $y \approx 0.4$ either from rock-salt type or from rutile-type structures. The optical absorption spectra of the films had two distinct components in regions of 0.44–2.4 eV and 2.4–6 eV, which arise from d–d and charge-transfer transitions, respectively. The former transition decreased with decreasing y and vanished at $y \approx 0.26$, where a fundamental absorption edge due to the latter transition was found to be 2.4 eV. The results demonstrate a range of anion compositions in the TiO_xN_y being suitable for visible-light harvesting applications.

INTRODUCTION

Photocatalytic water splitting is one of the important means to convert solar energy to hydrogen and other fuels.[1] TiO_2 is a popular photocatalytic material due to high photocatalytic activity, chemical stability, non-harmful nature, and low cost, and thus, it has been paid attention in decades.[2] However, TiO_2 has a drawback that photocatalytic reactions occur only under UV light owing to its wide bandgap, preventing practical solar-energy harvesting applications. The wide bandgap nature of TiO_2 originates from deep O 2p states, mainly composing valence band (VB), which largely overwhelms the oxidation potential of water. Therefore, it is effective to make the VB shallower by substitutional doping. In other words, new bonding states formed by a dopant are expected to appear above the O 2p states so that a band structure suitable to visible-light-driven water splitting is realized. For this purpose, the substitution of both Ti and O sites has been intensively studied.

A number of transition-metal elements are doped into TiO_2 to investigate the effect on visible-light absorption. Ghosh and Maruska reported a visible-light photoresponse of Cr-doped TiO_2 photoelectrodes.[3] The other transition-metal elements such as V, Fe, and Mo can also be doped. However, the substitution of the Ti sites generally decreases chemical stability or increases photoexcited carrier's recombination centers and, therefore, rather reduces the photocatalytic

activity.[4] As for the O sites, typical elements such as C,[5] N,[6–11] F,[12] and S[13] are attempted. Asahi *et al.* calculated the band structures of anatase TiO_2 doped with such elements and found that substitution with N atoms resulted in the shallower VB without forming in-gap states.[6] They also demonstrated a superior visible-light photocatalytic response for the N-doped TiO_2. Since then, various fabrication methods of N-doped TiO_2 films had been reported, for example, ammonolysis,[7] ion implantation,[8] sputtering in N_2/Ar mixed gas,[6] and others.[9–11] Chen *et al.* succeeded in fabricating heavily N-substituted anatase TiO_2 films (up to ≈15 at. %) using pulsed-laser deposition (PLD) with a TiN target.[11] They suggested that a solid N source was more effective than a gaseous source such as N_2 or NO for the incorporation of N atoms into TiO_2.

In order to further increase N content in titanates, it is effective to start from O-reduced phases such as TiO, Ti_2O_3, Ti_3O_5, and Ti_nO_{2n-1} ($n \geq 4$) because they can accommodate the N atom sites by changing the Ti valence to 4+.[14–21] For example, Hyett *et al.* synthesized a new titanium oxynitride (TiO_xN_y) phase by using a combinatorial chemical vapor deposition. They obtained $Ti_{3-\delta}O_4N$, whose crystal structure was monoclinic anosovite (β-Ti_3O_5).[22] They also verified higher photocatalytic performance of $Ti_{3-\delta}O_4N$ than TiO_2 under UV illumination (254 nm).[23] These results indicate that other TiO_xN_y act as effective photocatalysts under visible light. However, the previous studies focus on TiO_xN_y having only single compositions but various structures. Therefore, the N-content dependence of the structural and optical properties of TiO_xN_y has not been fully unveiled yet.

In this article, we report on systematic investigations on thin-film growth, crystal structure, and optical properties for TiO_xN_y films with various y. The TiO_xN_y films are epitaxially grown on α-Al_2O_3 (0001) substrates by using PLD with TiN as a solid-state N source. The N content in the films is tuned by changing O_2 pressure (P_{O2}) during the growth and analyzed by wavelength-dispersive x-ray fluorescence (XRF) spectroscopy. The crystal structure is found to change from rock-salt to rutile derivatives with increasing P_{O2}. The optical spectra for TiO_xN_y films exhibit two distinct components in the visible region, which evolve with y. We attribute them to intra-atomic d–d and charge-transfer (CT) transitions and discuss their contributions in terms of photoelectrochemically active visible-light absorption.

EXPERIMENTS

TiN, TiO_xN_y, and TiO_2 films were grown on α-Al_2O_3 (0001) substrates by using PLD equipped with a KrF excimer laser. The laser fluence and repetition rate for the ablation of TiN (TiO_2) were set as 2.0 (1.0) J cm^{-2} and 20 (20) Hz, respectively. The growth temperature was kept at 500 °C. The TiN film was fabricated using a TiN tablet (3N) under an N-radical atmosphere generated by a RF plasma source (400 W, 3×10^{-6} Torr). The TiO_xN_y films (Samples A–G) were fabricated using the TiN tablet under various P_{O2} (see Table I). The TiO_2 film was fabricated by using a TiO_2 single crystal (3N) under a P_{O2} of 1×10^{-3} Torr. The thickness of TiN and TiO_2 (TiO_xN_y) films was 40–50 (50–65) nm, which was measured by a stylus profiler.

The composition ratio of N/Ti (y) in the films was analyzed by XRF (ZSX Primus IV, Rigaku) using a TiN film as a standard.

TABLE I. Composition and the crystalline phase of TiO_xN_y films investigated in this study.

Sample	O_2 pressure (Torr)	y	Phase
A	1×10^{-5}	1.0	Rock salt
B	4×10^{-5}	0.51	Rock salt
C	6×10^{-5}	0.59	Rock salt
D	1×10^{-4}	0.42	Rock salt
E	4×10^{-4}	0.36	Distorted rutile
F	6×10^{-4}	0.29	Distorted rutile
G	1×10^{-3}	0.26	Distorted rutile

The structural and optical properties were investigated at room temperature by using x-ray diffraction (XRD) with Cu Kα_1 radiation and UV-vis-IR spectroscopy, respectively.

RESULTS AND DISCUSSION

As listed in Table I, y decreased with increasing P_{O2} during growth. This result demonstrates that the anion compositions can be controlled systematically by changing P_{O2}. Since the amount of N atoms ejected together with Ti atoms from the target is constant regardless of P_{O2}, N incorporation into the films is essentially suppressed by O_2 gas. This implies that for N atoms, the number of reaction sites available at the growing surface decreases with increasing P_{O2}. The composition of Sample A ($P_{O2} = 1 \times 10^{-5}$ Torr) was apparently the same as that of the target ($y \approx 1.0$), but XRD measurements revealed the presence of O atoms in this sample, as will be explained later. We noticed that O content x in the films could not be discriminated from that in the substrate by XRF analysis. In addition, unintentional incorporation at the interstitial sites as N_2 molecules and/or surface adsorbates of N species was inevitable in our experimental setup. The TiO_2 reference film grown by using a TiO_2 target under $P_{O2} = 1 \times 10^{-3}$ Torr indicated notably a large N signal ($y \approx 0.13$). In the following paragraphs, therefore, we carefully describe y and crystalline phases for Samples A–G to discuss their optical properties with respect to the reference films.

Figure 1 shows out-of-plane XRD profiles for films of Samples A–G, TiN, and TiO_2. The stoichiometric TiN film was obtained only when an N-radical source was employed. The TiN 111 reflection was detected at $2\theta \approx 36.7°$, which was consistent with the previous reports for a (111)-oriented TiN film grown on an α-Al_2O_3 (0001) substrate as well as a bulk one.[24,25] The film reflection of Sample A was detected at $2\theta \approx 37.3°$, which coincided with the TiO 111 reflection.[26] Taking near-unity y into account, this large lattice contraction from TiN (≈1.5%) is associated with the incorporation of O atoms. The rock-salt type lattice of $TiO_{1+\delta}$ ($-0.2 \leq \delta \leq 0.2$) is known to contract by 0.12% for every δ increment of 0.1.[27] Similar but the opposite tendency is reported for $TiN_{1-\delta}$ ($0 \leq \delta < 0.5$), where Ti is always rich, and the lattice contraction is also 0.12% for every δ increment of 0.1.[28] These facts suggest that Sample A is rock-salt type TiO_xN. Moreover, Laue fringes are seen clearly for the TiN film, and Sample A indicates good crystallinity and flat surface. Further verification of rock-salt type structures for Sample A will be described later.

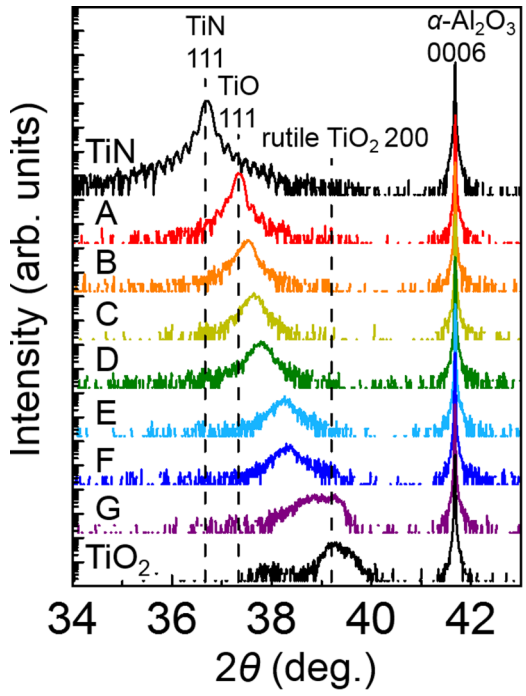

FIG. 1. Out-of-plane XRD profiles of TiO_xN_y films (Samples A–G). Those of TiN and TiO_2 films are also shown as references.

The film reflections for Samples B, C, and D were detected at $2\theta \approx 37.5°$, 37.6°, and 37.8°, respectively. These three films and Sample A indicated a systematic peak shift toward higher angles with increasing P_{O2}. Moreover, the peak intensity decreased gradually with P_{O2}, and the peak intensity for Samples D was smaller by an order of magnitude than that for Sample A. The diffuse reflections indicate increasingly pronounced disorder in the vicinity of structural transformation. The structural transformation was indeed seen with a large peak shift between Samples D ($y = 0.42$) and E ($y = 0.36$, $2\theta \approx 38.3°$). As will be described later, Samples E–G were tentatively assigned to be rutile derivatives from XRD measurements of asymmetric reflections. As for Sample F ($y = 0.29$), the film reflection appeared at the same angle as Sample E, suggesting the identical crystal structures to each other. Sample G also indicated diffuse reflection together with another one that coincided with the 200 reflection of rutile-type TiO_2, suggesting different orientations and/or compositional inhomogeneity. The reflection of the reference TiO_2 film was observed at $2\theta \approx 39.3°$, which was consistent with (100)-oriented rutile films grown on α-Al_2O_3 (0001).[29]

The overall peak shift of symmetric reflections for TiO_xN_y films can be understood from the oxidation states of Ti atoms. According to our previous study, the peak of titanate films grown on α-Al_2O_3 (0001) substrates tends to shift toward higher angle as the nominal valence of Ti increases from Ti^{2+} (TiO) to Ti^{4+} (TiO_2).[26] In addition, the lattice of rutile-type TiO_2 is known to expand as neutral O vacancies are incorporated,[30] implying that a reduced rutile film indicates a peak shift toward lower angle. In the present study, the film reflections systematically shifted toward higher angles as going from TiN (Ti^{3+}) to TiO_2 (Ti^{4+}).

XRD ϕ-scans were performed to Samples A–C with (111)-oriented rock-salt type structures. The asymmetric 200 reflections were taken at $2\theta \approx 44°$ and tilt angle $\chi \approx 57°$. As shown in Fig. 2, the in-plane rotational profiles exhibited a sixfold rotational symmetry, which was also seen for the $11\bar{2}3$ reflections of α-Al_2O_3 ($2\theta \approx 43.4°$ and $\chi \approx 61°$). This result revealed that Samples A–C had 180°-rotational domains. In addition, the in-plane epitaxial relationship was identified to be $TiO_xN_y\langle 11\bar{2}\rangle > //\alpha - Al_2O_3[11\bar{2}0]$, which was consistent with previous reports on TiN and TiO films grown on α-Al_2O_3 (0001) substrates.[24,26] As for Samples D–G, however, neither rock-salt 200 nor other asymmetric reflections were found. A highly disordered lattice suggested random distribution of N atoms including the interstitial sites. Nevertheless, the following issues can be deduced from systematic reflections shown in Fig. 1. The crystal structure of Samples D–G could be distinguished into two groups, rock-salt ($2\theta < 38°$) or rutile ($2\theta \approx 39°$) derived structures. Only Samples D would be in the former group. The others would be in the latter one because of common reflections at $2\theta \approx 38.3°$ for Samples F, G, and TiO_2. On the other hand, Samples E and F exhibited symmetric reflections at $2\theta \approx 38.3°$, which were unlike 200. According to our previous study, γ-Ti_3O_5 films grown on α-Al_2O_3 (0001) substrates show the 022 reflection at $2\theta \approx 38°$ that is located between TiO 111 and TiO_2 200 reflections in the out-of-plane XRD profile.[26,29] Since N incorporation into titanates leads to a lower-angle shift, a γ-Ti_3O_5 derived structure is excluded.

In order to fulfill an unambiguous assignment, we took diffraction patterns for Sample E using synchrotron radiation at the undulator beamline of BL15XU at SPring-8.[31] The photon energy

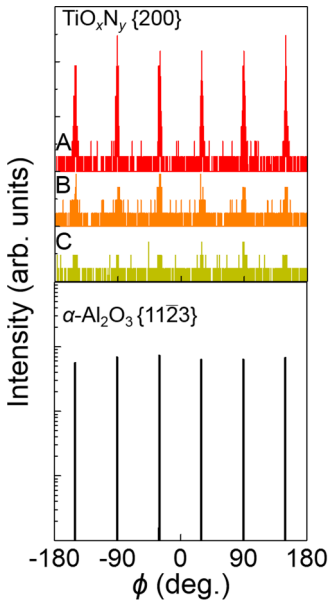

FIG. 2. XRD ϕ-scan profiles of TiO_xN_y 200 reflections for Samples A–C. A ϕ-scan profile of α-Al_2O_3 $11\bar{2}3$ reflections is also indicated as the reference.

of the grazing incident x-ray was set at 8.9 keV. The incidence and rocking angles were 1.5° and ±0.5°, respectively. Only film reflections were projected on an imaging plate placed opposite to the incident x-ray. A number of diffuse reflections were observed symmetrically with respect to the surface normal, and we tentatively assigned them to the rutile-type 220, 311, 321, and 421 because they were a set of particularly intense reflections for pure TiO_2. The same sets of diffuse spots were observed regardless of the azimuth angle, indicating no in-plane orientation. Given this correspondence, we assigned the symmetric reflection at $2\theta \approx 38.3°$ to rutile-type 210. The d spacing was evaluated to be 2.35 Å, which was exceptionally wide, more than 14% wider than that of pure TiO_2. Such an expansion is only known to the $CaCl_2$ type, a distorted rutile derivative. At the moment, severe disorder hampers further refinement of their crystal structures. Therefore, the crystalline phase of Samples E–G is referred to as distorted rutile (Table I).

Despite some ambiguity of the crystal structure, we have verified a visible-light photoresponse in the oxidation reaction of water. Three TiO_xN_y photoanodes (80-nm-thick) were prepared on 40-nm-thick TiN films grown on α-Al_2O_3 (0001) substrates under the same conditions for Samples E–G. Thus, these samples are referred to as Sample E′–G′. A reference TiO_2 photoanode was also prepared on a 0.5 wt. % Nb-doped TiO_2 (100) substrate. The samples were immersed in 0.1M NaOH aqueous solutions (pH = 13.0) with a Pt wire and a Ag/AgCl in 3M NaCl (E_0 = 0.203 V at 25 °C) that served as the counter and reference electrodes, respectively. The working electrodes were photoexcited by using a 500 W Xe lamp through a quartz window. Panchromatic and UV-cut visible light (≥422 nm) was irradiated during the linear sweep voltammetry. In contrast to TiO_2, anodic photocurrent was detected for Sample E′–G′ under visible light as well as Xe lamp illumination (Fig. 3). Moreover, a positive shift of onset potential by 0.55 V (1.05 V) was observed between TiO_2 and Sample G′ (Samples E′ and F′). This result strongly suggests the shallower VB in the TiO_xN_y.

Figure 4 shows the optical absorption spectra for the TiO_xN_y (Samples A–G) and TiO_2 films. The spectra for TiO_xN_y films had two distinct components in a range of photo energy, (i) 2.4–6 eV and (ii) 0.44–2.4 eV, which were attributed to CT and intra-atomic d–d transitions, respectively.[32] The onset of the absorption edge in the region (i) for the TiO_2 film was 3.3 eV, which was in good agreement with the bandgap (E_g) of rutile-type TiO_2.[33] In contrast, the onset of the absorption edge for all the TiO_xN_y films was nearly constant at ≈2.4 eV.[11] This is a striking finding because the CT gap, which is believed to arise mostly from N 2p to Ti 3d states,[6] is constant regardless of y and the crystalline phase. We plotted $(\alpha h\nu)^{1/2}$ as a function of $h\nu$, where α is the absorption coefficient and $h\nu$ is the photon energy, to estimate nearly constant E_g (≈2 eV).

Spectral weight in the region (ii) gradually decreased as going from Samples A to G, which was clearly seen as the change of film color (see the inset of Fig. 4) The color changed from dark black or blue (Samples A–D) to yellow (Sample G) via green (Samples E and F). TiO_2 indicated high transparency and no apparent feature arising from unintentionally incorporated N atoms. Taking the origin of d–d transitions into account, this tendency reflects the amount of electrons in Ti 3d bands. Gradual decreases in the 3d electrons and y are correlated to each other. In addition,

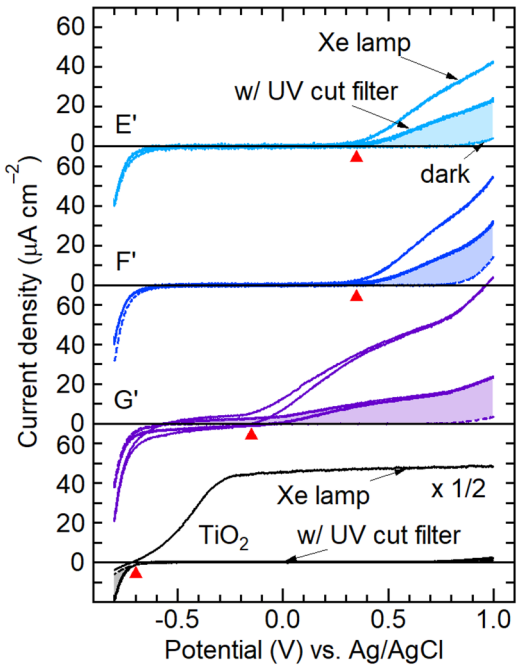

FIG. 3. Linear sweep voltammograms in the dark (dashed lines) and under panchromatic light (thin solid lines) and UV-cut visible light (bold solid lines) from a Xe lamp. The red triangles indicate the onset potentials of photoanodic current.

extrapolation toward lower $h\nu$ for Samples E–G predicts no absorption at 0 eV and thus their insulating nature. Meanwhile, Samples A–D show finite absorption at 0 eV that is a sign of the metallic state. We emphasize that Samples D and E have rock-salt and rutile-type structures, respectively, which is also captured by a discontinuous change of spectral weight in the region (ii).

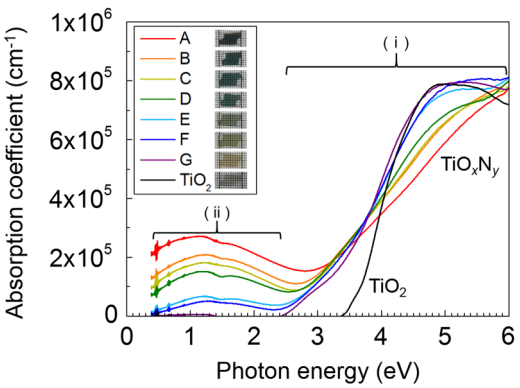

FIG. 4. Absorption spectra for TiO_xN_y (Samples A–G) and TiO_2 films (inset: optical images of the films, spacing of thin grid lines is 1 mm). The components in regions (i) and (ii) are responsible for CT and d–d transitions, respectively.

Figure 5 shows a difference in the absorption coefficient ($\Delta\alpha$) that is obtained by subtracting the absorption spectra of TiO_2 from those of Samples A–G. Now, spectral weight transfer can be clearly seen: the sign of $\Delta\alpha$ changes across $h\nu \approx 4$ eV. The negative part centered at ≈4.7 eV evolves as going from Samples G to A, which corresponds to damping of CT from O 2*p* to Ti 3*d* states because *x* (O/Ti) must decrease being opposite to increase in *y*. In contrast, the positive part shows two prominent components located at $h\nu \approx 1.2$ and 3.5 eV. The former is attributed to the *d*–*d* transition, and its evolution is perfectly associated with that of the negative part. The latter is attributed to the CT not only from N 2*p* to Ti 3*d* states, but also from O 2*p* to Ti 3*d* states. Moreover, their spectral shapes and magnitudes are almost constant regardless of anion compositions, suggesting a constant CT bandwidth.

The band diagram of TiO_xN_y films based on the optical spectra is illustrated in Fig. 6. Here, the origin of the horizontal axis is set to the bottom of the conduction band (CB). The Ti 3*d* states and N (O) 2*p* states are known to be hybridized in the VB for both TiN (TiO).[34] In contrast, CB predominately composes of Ti 3*d* states. As for TiO_2, CB and VB are mainly composed of Ti 3*d* and O 2*p* states, respectively. When N atoms were incorporated into TiO_2, N 2*p* states were formed ≈1 eV above the top of VB of TiO_2.[6] The arrows labeled with (i) and (ii) indicate CT and *d*–*d* transitions, respectively, which correspond to the regions (i) and (ii) in Fig. 4. Taking intact spectral feature centered at $h\nu \approx 3.5$ eV into account, N 2*p* and O 2*p* states at the top of VB almost equally contribute to the CT. In other words, the density of states (DOS) at the top of VB does not change significantly in a wide range of *y* (0.26–1.0). On the contrary, DOS of the lower *occupied* Ti 3*d* states does change significantly. Metallic behaviors found in Samples A–D suggest the presence of free carriers in the upper *unoccupied* Ti 3*d* states.

Our results indicate that a visible-light photocatalytic response is expected in a wide range of *y*. However, intra-atomic *d*–*d* transition usually does not contribute to the photocatalytic activity at all. We must elucidate an effective contribution of the visible-range CT. First, Sample G is superior to the others because *d*–*d* transition is absent. The absorption edge for Sample G is located at 2.4 eV. For quantitative analysis, we discriminated CT (2.4–3.3 eV) from

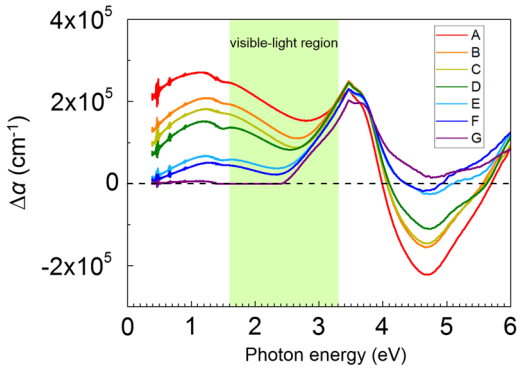

FIG. 5. Difference in absorption spectra of TiO_xN_y (Samples A–G) with respect to TiO_2.

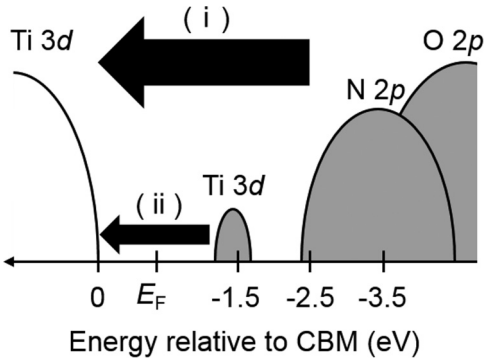

FIG. 6. Schematic band structure of TiO_xN_y. The arrows labeled with (i) and (ii) correspond to CT and *d*–*d* transitions, respectively.

total visible components (1.6–3.3 eV). Then, we took an integration of $\Delta\alpha$ in each region and defined them as S_{vis} and S_{CT}. Namely,

$$S_{vis} = \int_{1.6}^{3.3} \Delta\alpha(E)\mathrm{d}E \quad \text{and} \quad S_{CT} = \int_{2.4}^{3.3} \Delta\alpha(E)\mathrm{d}E,$$

where *E* is identical to $h\nu$. Figure 7 shows a central result of this study: values of S_{CT}/S_{vis} remain a constant when $y > 0.4$, while reach near unity at $y \approx 0.26$. This plot directly indicates that N content *y* has an optimum value for harvesting solar energy. When *y* exceeds the optimum value, CT in the UV region is cut; meanwhile, photocatalytically inactive *d*–*d* transition occurs (see Fig. 5).

In general, good photocatalytic water-splitting materials need to be insulating or semiconducting with a finite bandgap. Our samples with $0.42 \le y \le 1.0$ have a sufficient CT response (≈50% of visible light), but their metallic nature hampers photocatalytic applications. In contrast, Sample G ($y \approx 0.26$) is insulating, indicating neither *d*–*d* transition nor cut of CT in the UV region, to which one naturally

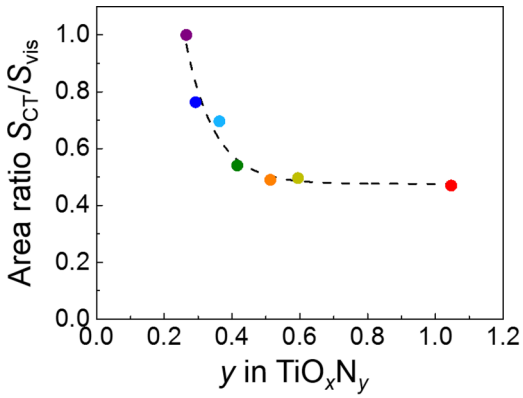

FIG. 7. N content dependence of S_{CT}/S_{vis} in TiO_xN_y films, indicating photoelectrochemically active fraction in the visible-light absorption. The dashed line is a guide for the eyes.

expects a nominal valence of Ti^{4+}. If so, oxygen content x can be reasonably assumed to be ≈1.6, and then the chemical formula is given by $TiO_{1.6}N_{0.26}$. This stoichiometry is similar to that of $Ti_8O_{13}N_2$, which is regarded as N-substituted Ti_7O_{13}, a member of Magnéli phase Ti_nO_{2n-1} ($n = 8$). The Magnéli phases have low-dimensional structures characterized by crystallographic shear planes that amputate the edge-shared infinite TiO_6 chains at ever n TiO_6 blocks. The nominal valence of Ti^{4+} remains only if three O atoms in Ti_nO_{2n-1} are substituted by two N atoms (i.e., $Ti_nO_{2n-3}N_2$). In this regard, n corresponds to 5–7 for insulating Samples E ($y \approx 0.36$) and F ($y \approx 0.29$). Even if so, x does not necessarily follow to keep Ti^{4+}, as they show clear d–d transition (Figs. 4 and 5). In addition, lattice disorder will be increasingly pronounced with decreasing n due to higher density shear planes. Therefore, small amounts of N atoms are advantageous not only to visible-light excited CT, but also to high-mobility diffusion of photoexcited carriers.

In other aspects, well-known Ti nitrides such as TiN and Ti_2N are metallic, and they cannot be applied to photocatalysts for water splitting. In recent years, a higher titanium nitride Ti_3N_4 has been synthesized at ultrahigh pressure and temperature. However, it is theoretically predicted as a narrow gap semiconductor ($E_g = 0.8$–0.9 eV) and unstable at ambient pressure and temperature.[35] Our samples were stable in air in the course of months. Among the Ti compounds, therefore, titanium oxynitrides are one of a few promising candidates for visible-light-driven water splitting.

CONCLUSION

In conclusion, we fabricated TiO_xN_y films with various N contents on α-Al_2O_3 (0001) substrates by using PLD with a TiN ceramic target as an N source. The N content y in the films decreased with increasing P_{O2}. The crystalline phase transformed from a rock-salt type to rutile derivatives as y exceeded 0.4. The optical absorption spectra for TiO_xN_y films had two distinct structures in the regions below and above 2.4 eV, which were attributed to intra-atomic d–d and CT transitions, respectively. Incorporation of the larger amount of N atoms resulted in an increasing contribution of the d–d transition. Taking photoelectrochemically inactive d–d transition into account, we conclude that the small amount of N atoms, where the rutile-like structure is preserved, is beneficial for relatively large CT absorption in the visible region.

ACKNOWLEDGMENTS

The authors thank Jun-ichi Yamaura for preliminary synchrotron XRD measurements at KEK-PF. The synchrotron XRD measurements were performed under the approval of the NIMS Synchrotron X-ray Station at SPring-8 (Proposal Nos. 2017A4700 and 2019A4702). The authors also thank Y. Katsuya for technical support. This work was partly supported by MEXT Element Strategy Initiative to Form Core Research Center (Grant No. JPMXP0112101001) and a Grant-in-Aid for Scientific Research (Nos. 18H03925 and 19H02588) from the Japan Society for the Promotion of Science Foundation.

REFERENCES

[1] A. Fujishima and K. Honda, Nature **238**, 37 (1972).
[2] A. Fujishima, X. Zhang, and D. Tryk, Surf. Sci. Rep. **63**, 515 (2008).
[3] A. K. Ghosh and H. P. Maruska, J. Electrochem. Soc. **124**, 1516 (1977).
[4] W. Choi, A. Termin, and M. R. Hoffmann, J. Phys. Chem. **98**, 13669 (1994).
[5] H. Irie, Y. Watanabe, and K. Hashimoto, Chem. Lett. **32**, 772 (2003).
[6] R. Asahi, T. Morikawa, T. Ohwaki, K. Aoki, and Y. Taga, Science **293**, 269 (2001).
[7] H. Irie, Y. Watanabe, and K. Hashimoto, J. Phys. Chem. B **107**, 5483 (2003).
[8] A. Ghicov, J. M. Macak, H. Tsuchiya, J. Kunze, V. Haeublein, L. Frey, and P. Schmuki, Nano Lett. **6**, 1080 (2006).
[9] H. Matsui, H. Tabata, N. Hasuike, H. Harima, and B. Mizobuchi, J. Appl. Phys. **97**, 123511 (2005).
[10] T. Morikawa, R. Asahi, T. Ohwaki, K. Aoki, and Y. Taga, Jpn. J. Appl. Phys. **40**, L561 (2001).
[11] T. L. Chen, Y. Hirose, T. Hitosugi, and T. Hasegawa, J. Phys. D: Appl. Phys. **41**, 062005 (2008).
[12] J. C. Yu, J. Yu, W. Ho, Z. Jiang, and L. Zhang, Chem. Mater. **14**, 3808 (2002).
[13] T. Umebayashi, T. Yamaki, H. Itoh, and K. Asai, Appl. Phys. Lett. **81**, 454 (2002).
[14] N. J. Doyle, J. K. Hulm, C. K. Jones, R. C. Miller, and A. Taylor, Phys. Lett. A **26**, 604 (1968).
[15] C. N. R. Rao, R. E. Loehman, and J. M. Honig, Phys. Lett. A **27**, 271 (1968).
[16] S. Åsbrink and A. Magnéli, Acta Crystallogr. **12**, 575 (1959).
[17] H. Iwasaki, N. F. H. Bright, and J. F. Rowland, J. Less-Common Met. **17**, 99 (1969).
[18] S. H. Hong and S. Åsbrink, Acta Crystallogr. Sect. B **38**, 2570 (1982).
[19] M. Onoda, J. Solid State Chem. **136**, 67 (1998).
[20] S. Ohkoshi, Y. Tsunobuchi, T. Matsuda, K. Hashimoto, A. Namai, F. Hakoe, and H. Tokoro, Nat. Chem. **2**, 539 (2010).
[21] M. Marezio, D. B. Mcwhan, P. D. Dernier, and J. P. Remeika, J. Solid State Chem. **6**, 213 (1973).
[22] G. Hyett, M. A. Green, and I. P. Parkin, J. Am. Chem. Soc. **129**, 15541 (2007).
[23] G. Hyett, M. A. Green, and I. P. Parkin, J. Photochem. Photobiol. A **203**, 199 (2009).
[24] V. Talyansky, R. D. Vispute, R. Ramesh, R. P. Sharma, T. Venkatesan, Y. X. Li, L. G. Salamanca-Riba, M. C. Wood, R. T. Lareau, K. A. Jones, and A. A. Iliadis, Thin Solid Films **323**, 37 (1998).
[25] N. Pessall, R. E. Gold, and H. A. Johansen, J. Phys. Chem. Solids **29**, 19 (1968).
[26] H. Kurokawa, K. Yoshimatsu, O. Sakata, and A. Ohtomo, J. Appl. Phys. **122**, 055302 (2017).
[27] J. K. Hulm, C. K. Jones, R. A. Hein, and J. W. Gibson, J. Low Temp. Phys. **7**, 291 (1972).
[28] N. J. Ashley, R. W. Grimes, and K. J. McClellan, J. Mater. Sci. **42**, 1884 (2007).
[29] C. Wang, J. Dho, and S. G. Lee, J. Cryst. Growth **380**, 118 (2013).
[30] B. Santara, P. K. Giri, K. Imakita, and M. Fujii, J. Phys. D: Appl. Phys. **47**, 215302 (2014).
[31] M. Tanaka, Y. Katsuya, and O. Sakata, AIP Conf. Proc. **1741**, 050019 (2016).
[32] Y. Okimoto, T. Katsufuji, Y. Okada, T. Arima, and Y. Tokura, Phys. Rev. B **51**, 9581 (1995).
[33] V. N. Kuznetsov and N. Serpone, J. Phys. Chem. C **113**, 15110 (2009).
[34] V. Ern and A. C. Switendick, Phys. Rev. **137**, A1927 (1965).
[35] V. S. Bhadram, H. Liu, E. Xu, T. Li, V. B. Prakapenka, R. Hrubiak, S. Lany, and T. A. Strobel, Phys. Rev. Mater. **2**, 011602 (2018).